PNAS

Supporting Information for
Macrophages modulate stiffness-related foreign body responses through plasma membrane deformation

Yueqi Ni[1,3], Haoning Qi[1,3], Fanyu Zhang[1], Shuting Jiang[1], Qinchao Tang[1], Wenjin Cai[1], Wenting Mo[1], Richard J Miron[1], Yufeng Zhang[1,2*]

1 The State Key Laboratory Breeding Base of Basic Science of Stomatology (Hubei MOST)& Key Laboratory of Oral Biomedicine Ministry of Education School and Hospital of Stomatology Wuhan University, Wuhan 430079, China.

2 Medical Research Institute, School of Medicine, Wuhan University, Wuhan 430071, China.

3 These authors contributed equally to this work

*Corresponding author: Yufeng. Zhang

Email: zyf@whu.edu.cn

This PDF file includes:

Figures S1 to S8
Tables S1

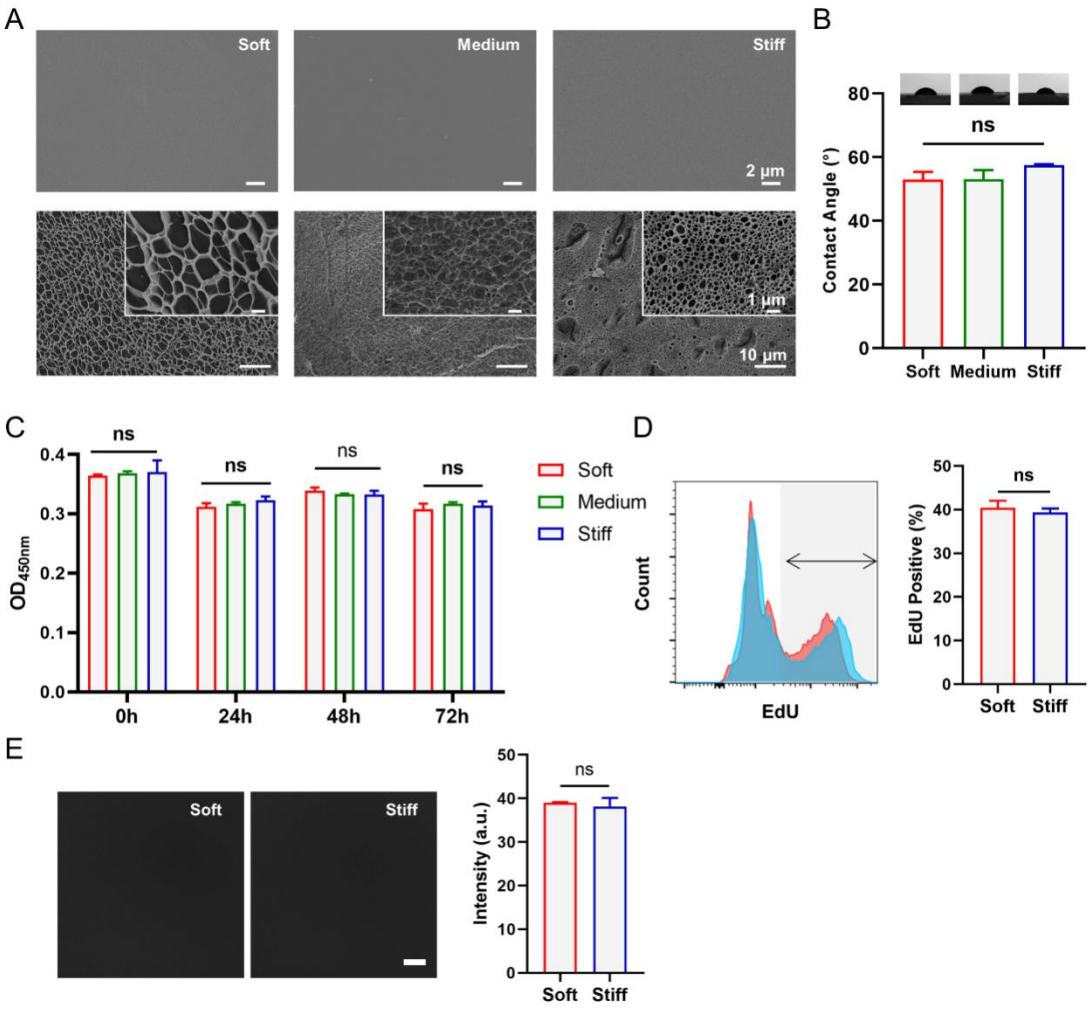

Supplementary Fig. 1 (A) SEM images of PVA hydrogels. Hydrogels were frozen in liquid nitrogen and then freeze-dried in a vacuum freeze-dryer for 24 h, indicating differences in pore size (lower images). However, the micron-sized pores observed by directly dewatering in a vacuum freeze-dryer overnight are largely due to the dehydration method (upper images). (B) Statistical analysis of the water contact angle of PVA hydrogels (*n*=3). One-way ANOVA with Tukey's posttest. (C) Analysis of CCK8 test results of BMDMs cultured on PVA hydrogels. One-way ANOVA with Tukey's posttest. (D) Analysis of the cell proliferation ratio detected by flow cytometry (*n*=3). Two-tailed Student's t-test. (E) Representative immunofluorescence images and fluorescence intensity statistics of PVA hydrogels with different stiffnesses incubated with 10 μg/ml FITC-RGD on the surface, showing a uniform distribution of ligands on the hydrogel surface and no difference in adsorption amount (*n*=3). Two-tailed Student's t-test. * $P < 0.033$, ** $P < 0.002$, *** $P < 0.001$; *ns*, no significant difference.

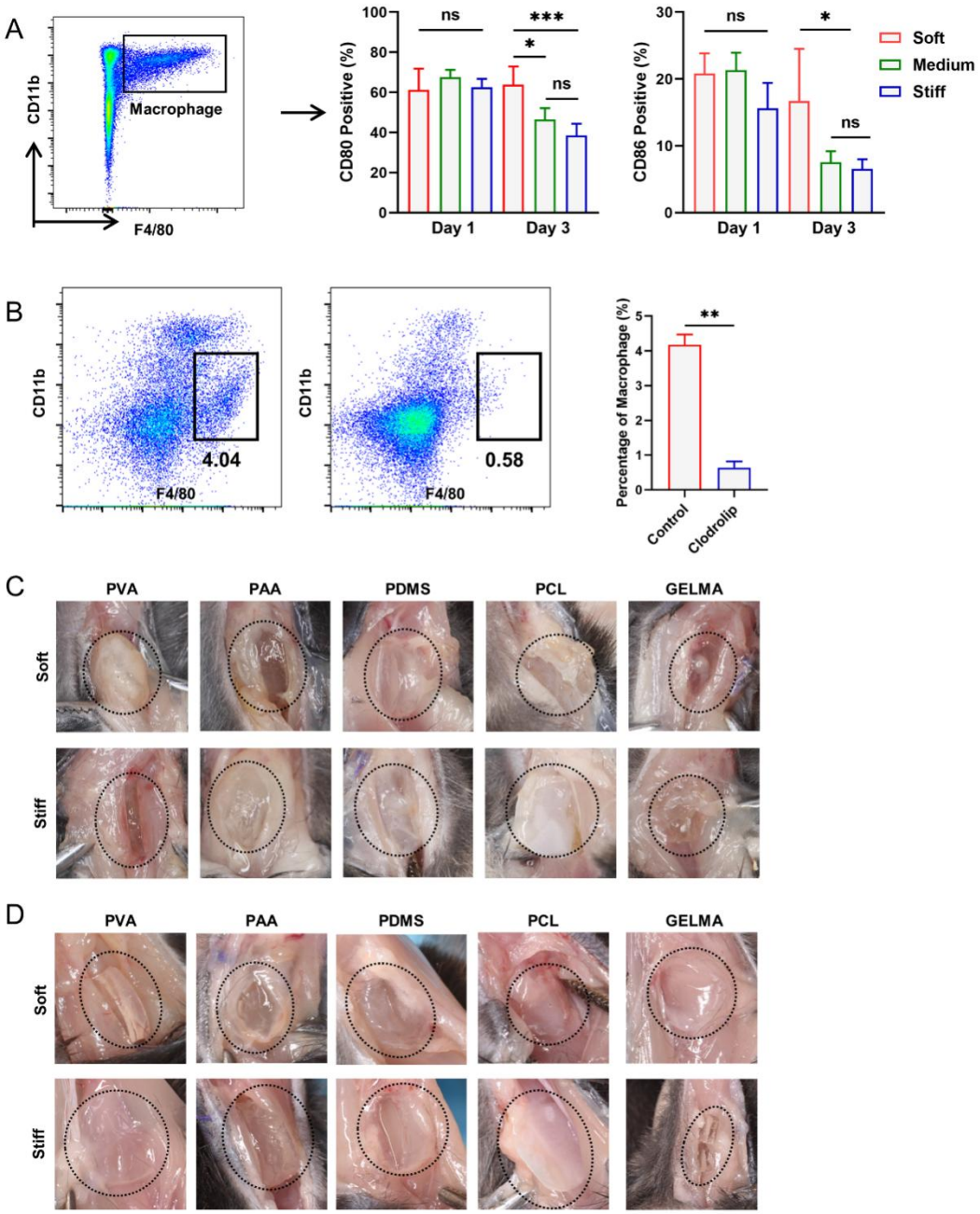

Supplementary Fig. 2 (A) Flow cytometry analysis of implantation site tissue one day and three days after PVA hydrogel implantation in mice (*n*=4; * *P*=0.04, * *P*=0.02). One-way ANOVA with Tukey's posttest. (B) Macrophage liposome clearance efficiency was measured by flow cytometry results of the percentage of splenic macrophages in mice one day after tail vein injection (*n*=5; ** *P*=0.0079). Nonparametric test. (C) Representative images of fibrosis at the implantation site 14 days after surgery in mice, showing differences in fibrosis mediated by implant stiffness. (D) Representative images of fibrosis at the implantation site 14 days after implantation surgery in mice undergoing macrophage clearance, demonstrating differences in fibrosis mediated by

reduced implant stiffness and decreased cell deposition. * $P < 0.033$, ** $P < 0.002$, *** $P < 0.001$; *ns*, no significant difference.

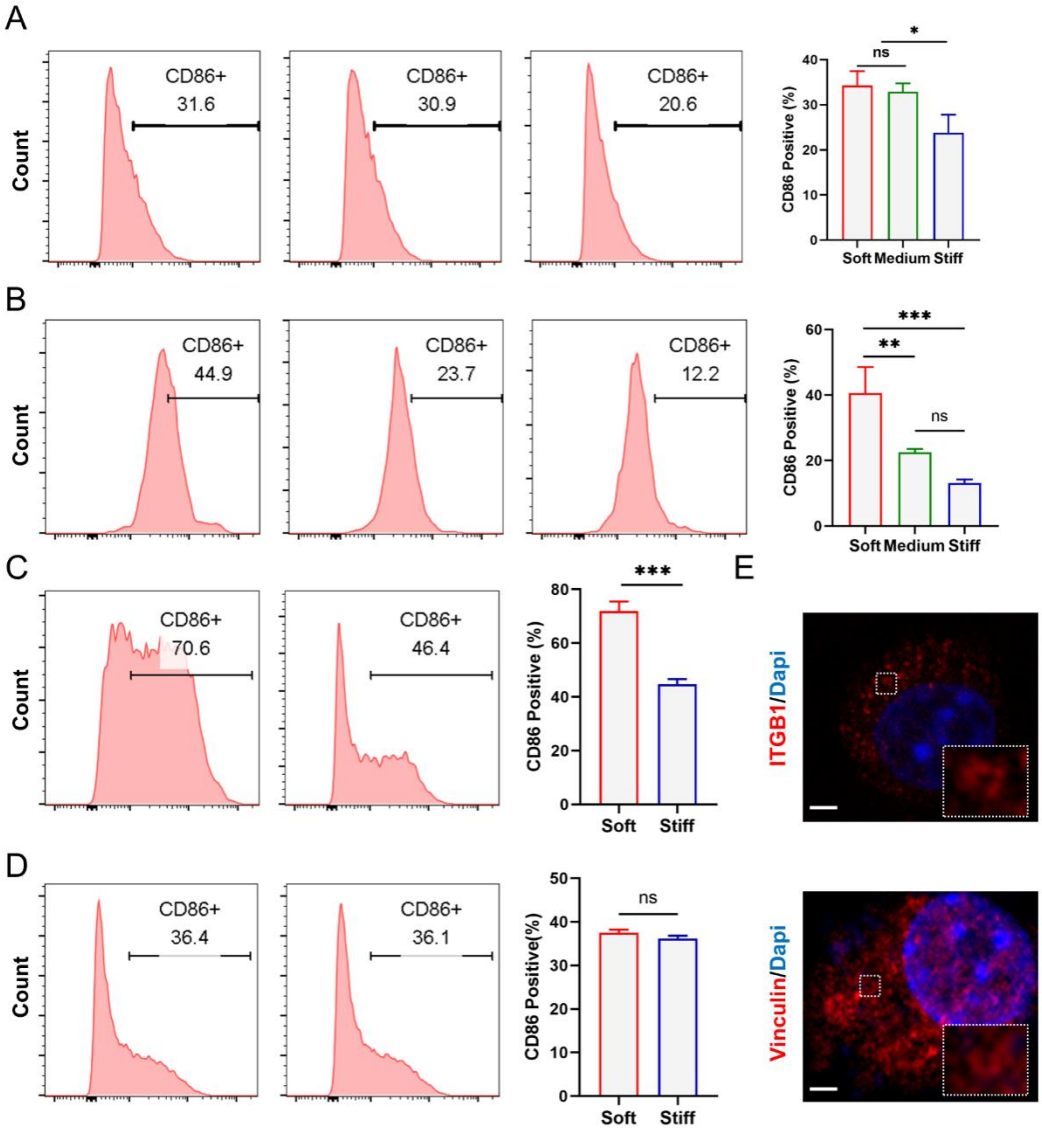

Supplementary Fig. 3 (A) Flow cytometry analysis of RAW264.7 cells cultured on PVA hydrogels for 24 h (n=3; * P=0.02, * P=0.03). (B) Flow cytometry analysis of BMDMs cultured on PVA hydrogels for 24 h (n=3; ** P=0.008). (C) Flow cytometry analysis of RAW264.7 cells cultured on PAA hydrogels for 24 h (n=3). Two-tailed Student's t-test. (D) Flow cytometry analysis of RAW264.7 cells cultured on PDMS hydrogels for 24 h (n=4). Two-tailed Student's t-test. (E) Representative confocal images of RAW264.7 cells. The local wraparound distribution of vinculin and ITGB1 suggests that integrins in macrophages are mainly involved in the formation of podosomes, in which an adhesion complex forms an annulus. Nuclei are blue, and Integrin and Vinculin are red. Scale bar, 2 μm. Data were analyzed by one-way ANOVA with Tukey's posttest. * P < 0.033, ** P < 0.002, *** P < 0.001; *ns*, no significant difference.

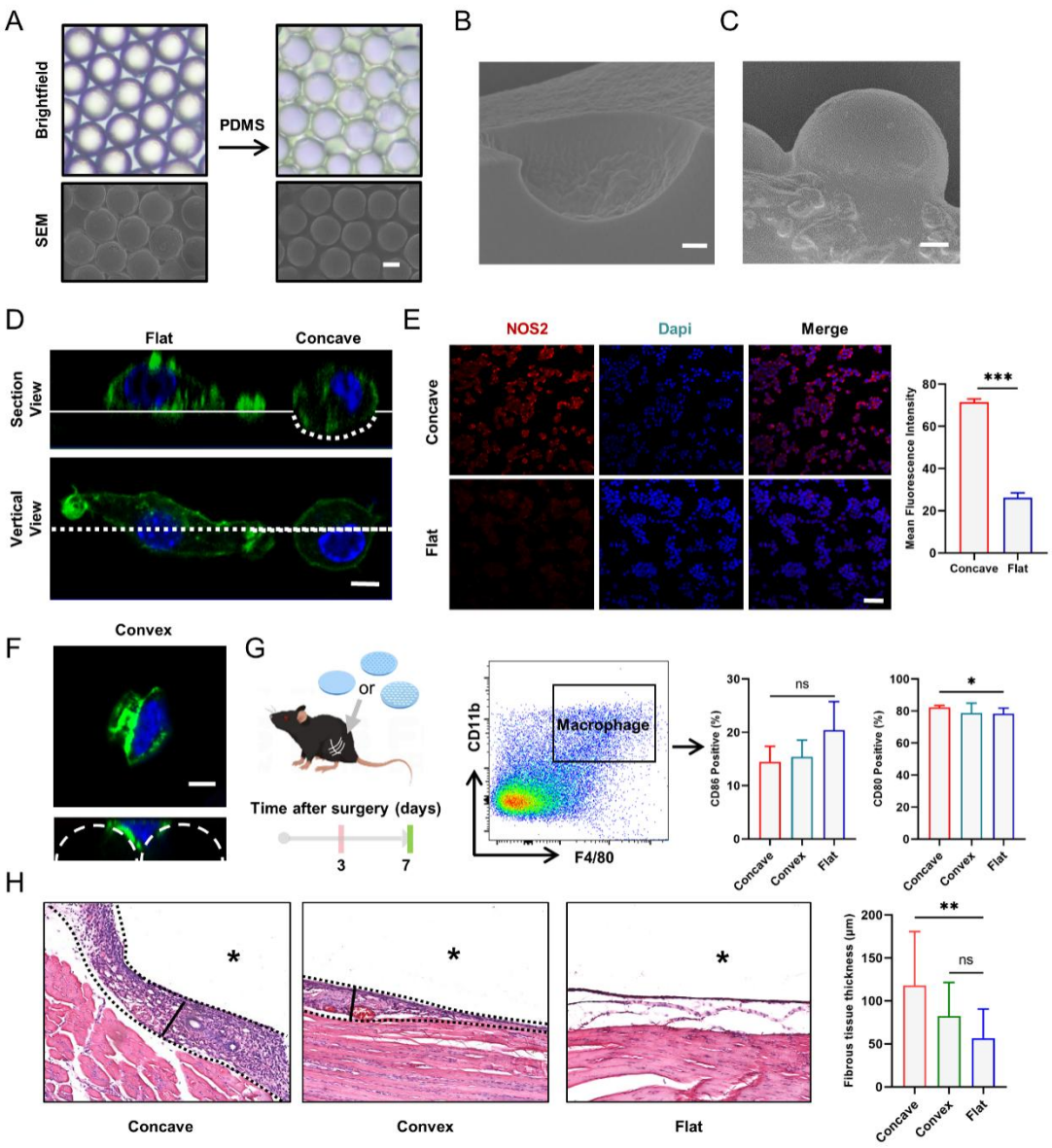

Supplementary Fig. 4 (A) SEM and bright-field images of the self-assembled polystyrene microspheres (left) and the final obtained processed concave surface. Scale bar, 10 μm. (B) SEM image of concave depth. Scale bar, 2 μm. (C) SEM image of the vertical view of convex. Scale bar, 2 μm. (D) Representative confocal images of RAW264.7 cells cultured on the flat substrate and concave substrate demonstrate the expected plasma membrane deformation due to surface topography. F-actin is green, and nuclei are blue. Scale bar, 5 μm. (E) Representative confocal images and the analysis of the fluorescence intensity of NOS2. NOS2 is red, nuclei are blue. Scale bar, 50 μm. Two-tailed Student's t-test. (F) Representative confocal images of RAW264.7 cells cultured on the convex substrate demonstrate the plasma membrane deformation due to surface topography. F-actin is green, and nuclei are blue. Scale bar, 5 μm. (G) Schematic of implant surgery of different topography PDMS implanted in the quadriceps muscle group of mice

and the experimental timeline. Flow cytometry analysis of implantation site tissue three days after PDMS implantation in mice (n=4; * P=0.0462). One-way ANOVA with Tukey's posttest. (H) Quantification of the variation in fibrous capsule thickness with material topography by H&E staining (n=15; ** P = 0.002). One-way ANOVA with Tukey's posttest. * P < 0.033, ** P < 0.002, *** P < 0.001; *ns*, no significant difference.

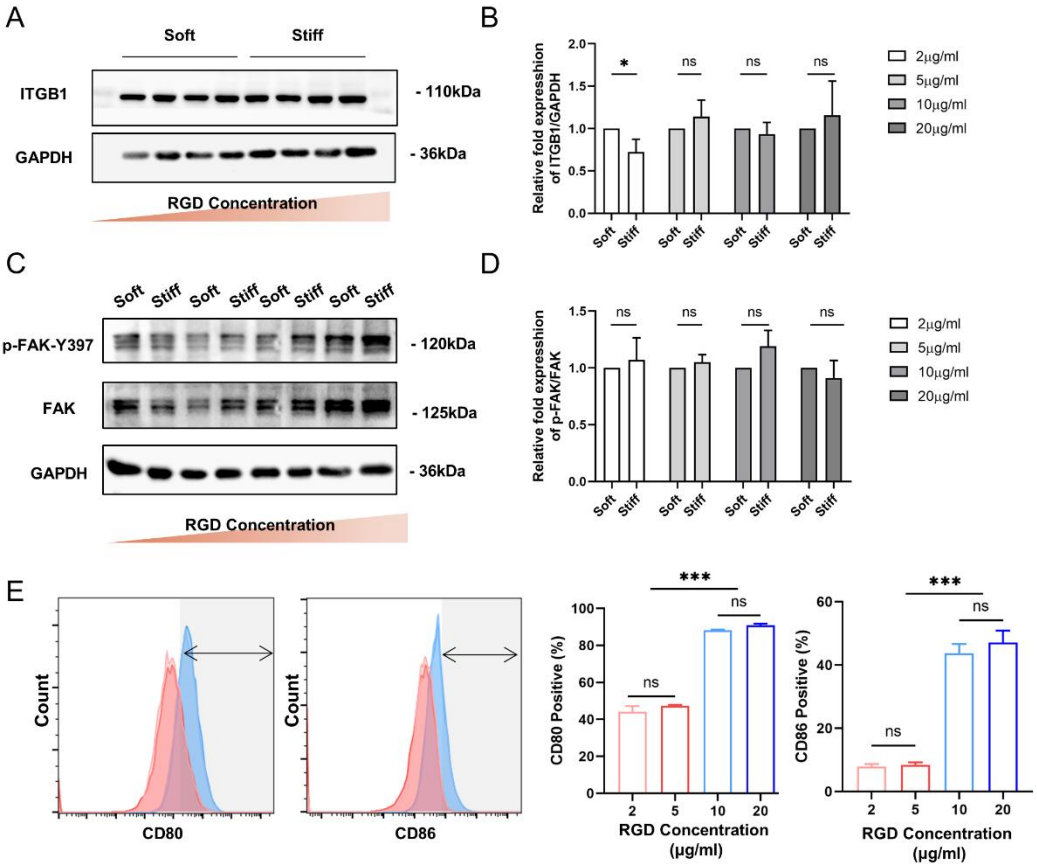

Supplementary Fig. 5 (A-D) No significant difference in ITGB1 and p-FAK-Y397 expression on soft and stiff substrates with increasing ligand concentration (*n*=3; * *P*=0.0343). Two-tailed Student's t-test. (E) Flow cytometry analysis of RAW264.7 cells cultured in cell culture dishes incubated with different concentrations of ligands for 24 h, suggesting that high concentrations of ligands promote inflammatory activation of macrophages. * $P < 0.033$, ** $P < 0.002$, *** $P < 0.001$; *ns*, no significant difference.

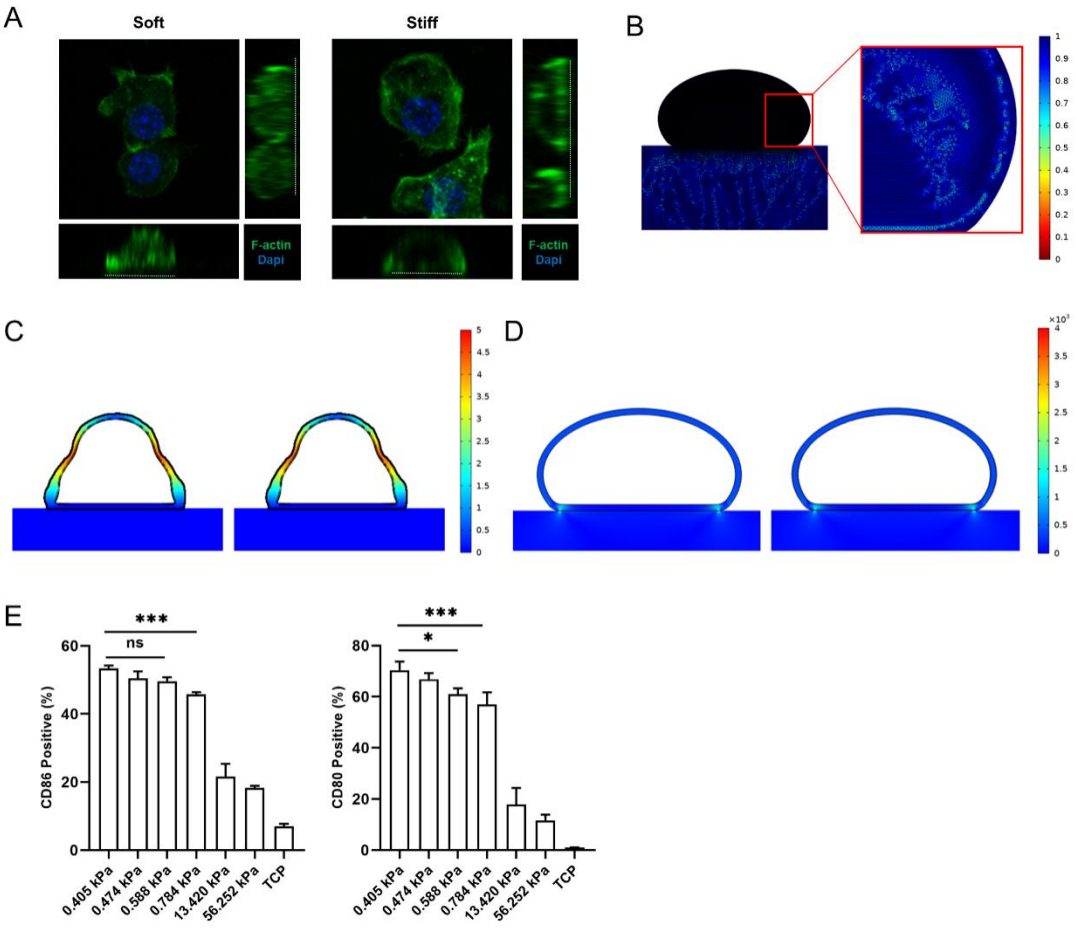

Supplementary Fig. 6 (A) Orthogonal view of z-stack images of macrophages cultured on PDMS for 2 hours. F-actin is green, and nuclei are blue. Scale bar, 5 μm. (B) Schematic diagram of the gridding of cell-substrate models. The color scale represents the size of the grid unit. (C) Displacement of the cell membrane with different stiffnesses of the PDMS substrate, with the color scale illustrating the displacement size (μm). (D) Von Mises equivalent strains of the cell membrane periphery with different stiffnesses of the PDMS substrate, with the color scale illustrating the stress magnitude (N/m2). (E) Flow cytometry analysis of RAW264.7 cells cultured on different stiffness PVA hydrogels for 24 h (n=4; * P = 0.02). Two-tailed Student's t-test. * P < 0.033, ** P < 0.002, *** P < 0.001; *ns*, no significant difference.

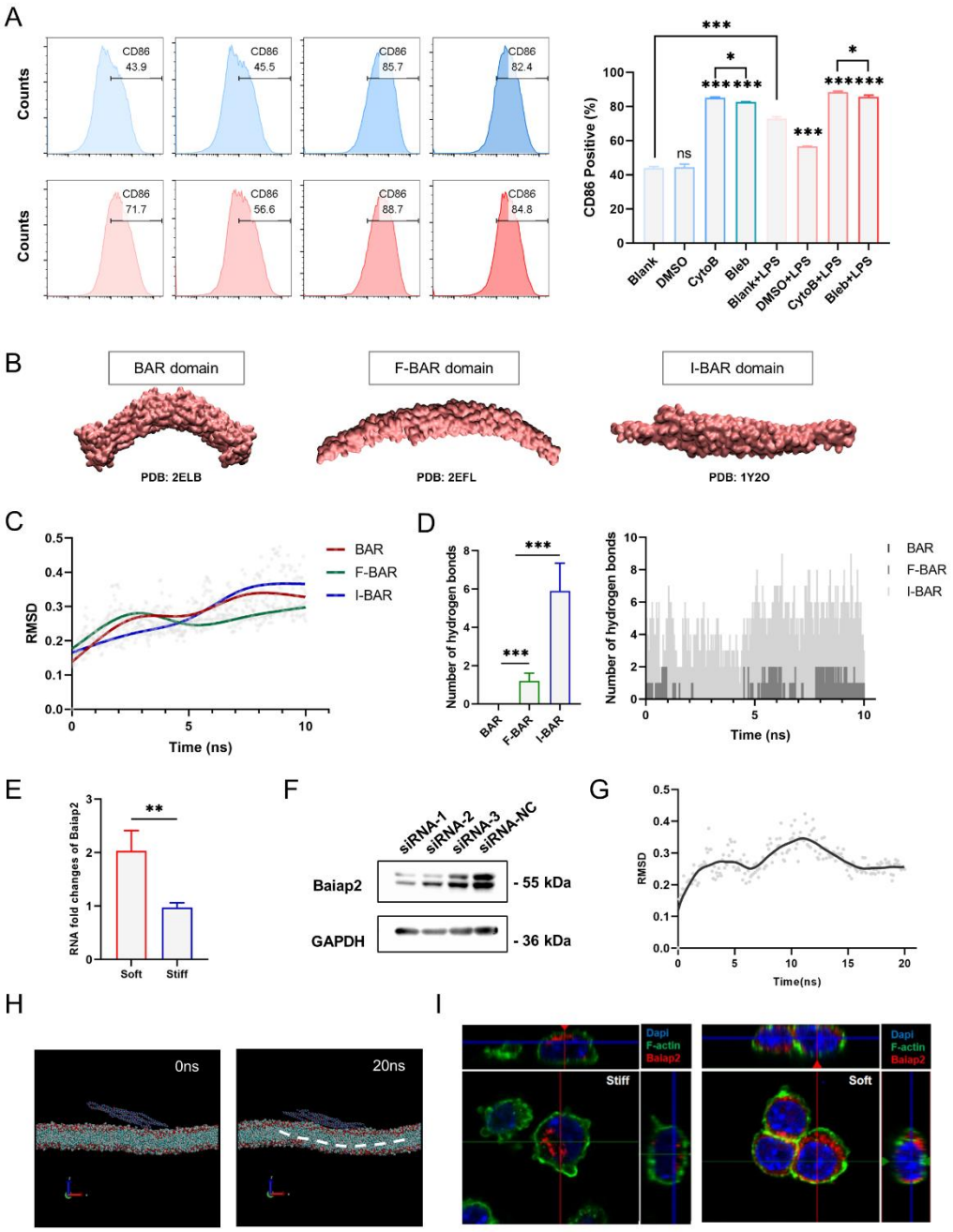

Supplementary Fig. 7 (A) Flow cytometry analysis of the contribution of actin and myosin to inflammatory activation in macrophages (n=3; * P=0.05, * P=0.03) (B) Representative images of three BAR subfamily domains rendered by VMD. (C) Root mean squared error (RMSD) of the proteins in three molecular dynamics simulations. (D) The analysis and the evolution of the number of hydrogen bonds between the proteins and membrane during the 10-ns simulation. (E) Gene expression of RAW264.7 cultured on different substrates for 2 h (n=3; ** P=0.01). Data were assessed using a two-tailed Student's t-test. (F) The expression of Baiap2 after a

knockdown by siRNA. (G) RMSD of the I-BAR domain and membrane during the 20-ns simulation. (H) Representative images of the interaction between the I-BAR domain and membrane during 20-ns simulation. (I) Orthogonal view of z-stack images of macrophages cultured on PVA hydrogels for 2 h. Baiap2 is red, f-actin is green, and the nuclei are blue. Scale bar, 5 μm. Data were analyzed by one-way ANOVA with Tukey's posttest. * $P < 0.033$, ** $P < 0.002$, *** $P < 0.001$; *ns*, no significant difference.

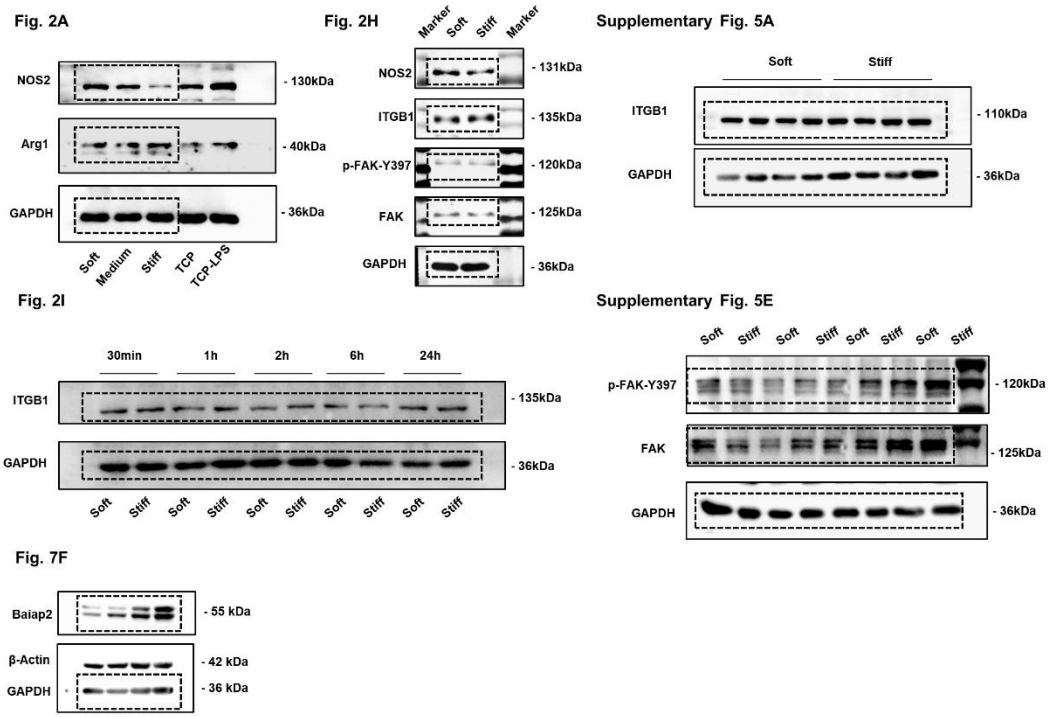

Supplementary Fig. 8

Supplementary. Table 1. Primer Sequences

Gene	Forward Sequence（5’-3’）	Reverse Sequence（5’-3’）
NOS2	GGAGTGACGGCAAACATGACT	TCGATGCACAACTGGGTGAAC
IL-1β	GCAACTGTTCCTGAACTCAACT	ATCTTTTGGGGTCCGTCAACT
TNF-α	TGTCTCAGCCTCTTCTCATT	TGATCTGAGTGTGAGGGTCT
CD80	ACCCCCAACATAACTGAGTCT	TTCCAACCAAGAGAAGCGAGG
IL-6	ACTGATGCTGGTGACA	GCAAGTGCATCATCGT
CD86	TGTTTCCGTGGAGACGCAAG	TTGAGCCTTTGTAAATGGGCA
GAPDH	AGGTCGGTGTGAACGGATTTG	TGTAGACCATGTAGTTGAGGTCA
Baiap2	ATGTCGCTTTCACGCTCGG	ATGGCGATGAAGTTGCGGA